scientific reports

Check for updates

OPEN

Morphologic characteristics of distal intracranial arteries in relation to structural changes in the brain after chronic alcohol consumption

Cuiqin Wang[1], Yanjie Jia[1]✉, Longbin Jia[2], Lina Xu[2], Fengbing Yang[2], Jinna Li[2], Hongjiang Cheng[2], Huanhuan Cui[2], Jing Guo[3], Jianqiang Wang[4] & Chong Li[4]

This study focuses on the structural brain changes, alterations in Apparent Diffusion Coefficient (ADC) values, and the morphological characteristics of distal intracranial arteries in chronic alcohol consumption. A total of 50 chronic alcoholics and 43 non-alcoholics were recruited from neurology inpatient and outpatient services. Using the Brainnetome Atlas to segment the brain into 246 regions, ADC values were observed to be consistently higher in alcoholics, with statistically significant differences in 134 of these regions. This number is far greater than the number of brain regions where changes in gray matter volume were observed. The alcohol group exhibited lower mean arterial density, mean arterial radius, and mean arterial tortuosity, along with higher mean arterial flexibility, though mean arterial length did not differ significantly between groups. But correlation analysis revealed a negative relationship between alcohol consumption and mean arterial density and mean arterial length. Gray matter volume was positively correlated with mean arterial length, density, and radius. White matter volume also showed a positive correlation with mean arterial length and density. Conversely, cerebrospinal fluid volume was negatively correlated with mean arterial length and density. These results suggest that the diffusion of water molecules in the brains of alcoholics is altered before observable changes in gray matter structure occur. Changes in cerebrovascular morphology are a contributing factor to the structural brain changes observed in chronic alcoholics.

Keywords Chronic alcohol consumption, Structural brain changes, ADC measurements, Morphological characterization, Distal intracranial arteries

Abbreviations

MRI	Magnetic resonance imaging
MRA	Magnetic resonance angiography
ADC	Apparent diffusion coefficient
VBM	Voxel-based morphometry
SBM	Surface-based morphology
DWI	Diffusion-weighted imaging
DTI	Diffusion tensor imaging
TIV	Total intracranial volume
GMV	Gray matter volume
WMV	White matter volume
CSFV	Cerebrospinal fluid volume
WMH	Cerebral white matter high signal volume
MCV	Mean corpuscular volume

[1]Department of Neurology, The First Affiliated Hospital of Zhengzhou University, Zhengzhou, Henan Province, China. [2]Department of Neurology, Jincheng City People's Hospital, Jincheng, Shanxi Province, China. [3]Department of Laboratory, Jincheng City People's Hospital, Jincheng, Shanxi Province, China. [4]Department of Imaging, Jincheng City People's Hospital, Jincheng, Shanxi Province, China. ✉email: jiayanjie1971@zzu.edu.cn

MCH	Mean corpuscular hemoglobin
MCHC	Mean corpuscular hemoglobin concentration
ALT	Alanine aminotransferase
AST	Aspartate transaminase
PT	Prothrombin time
PTA	Prothrombin activity
INR	International normalized ratio
FIB	Fibrinogen
TT	Thrombin time
APTT	Activated partial thromboplastin time
HDL	High-density lipoprotein
LDL	Low-density lipoprotein
FT3	Free triiodothyronine
FT4	Free thyroxine
TSH	Thyroid-stimulating hormone
AUDIT	Alcohol use disorders identification test
PSQI	Pittsburgh sleep quality index
MMSE	Mini-mental State Examination
MoCA	Montreal cognitive assessment
IL-1b	Interleukin-1b
IL-2	Interleukin-2
IL-4	Interleukin-4
IL-6	Interleukin-6
IL-10	Interleukin-10
TNF-α	Tumor necrosis factor-α
INF-γ	Interferon-γ
GFAP	Glial fibrillary acidic protein
NFL	Neurofilament light chain
sTREM2	Soluble Triggering receptor expressed on myeloid cells 2
HCP-MMP1	Human Connectome Project Multi-modal Parcellation 1.0
MCA	Middle cerebral artery
ACA	Anterior cerebral artery
PCA	Posterior cerebral artery
FA	Fractional anisotropy
MD	Mean diffusivity
MK	Mean kurtosis
MSA-P	Multiple system atrophy-P
mL	Milliliter
STL	Stereolithrography

Extensive brain atrophy in alcohol-dependent individuals (ALC) has been consistently documented in both pathological and magnetic resonance imaging (MRI) studies[1]. MRI research provides compelling evidence that chronic alcohol consumption results in significant alterations in gray and white matter[2]. Chronic heavy drinking predominantly impacts the frontal lobe, mesencephalon, hippocampus, and cerebellar structures. A negative correlation has been observed between alcohol intake and overall brain volume, regional gray matter volume, and white matter microstructure[3]. Recently, Zhou et al. (2024) conducted a meta-analysis of structural MRI studies and further confirmed the relationship between long-term alcohol consumption and brain atrophy, providing more comprehensive evidence for this well-established finding[4]. In studies examining alcohol use and brain development in adolescents, findings revealed that alcohol consumption is associated with thinner total, frontal, temporal, and cingulate cortices compared to non-drinkers[5]. Higher levels of alcohol consumption correlate with multiple markers of white matter microstructure, including reduced fractional anisotropy and increased mean and radial diffusivity, with a widespread distribution across the brain[6].

Voxel-based morphometry (VBM) is an automated, comprehensive, and objective technique for voxel-based analysis of brain structures via magnetic resonance imaging (MRI), allowing for the quantitative calculation and analysis of gray and white matter density or volume changes in each voxel, thereby highlighting differences in corresponding anatomical structures[7]. Surface-based morphology (SBM) offers a computational approach to MR imaging data, quantifying the brain's gray matter morphological structure through parameters such as thickness, surface area, volume, and curvature[8].

In this study, VBM analysis was employed to obtain measurements of gray matter volume, white matter volume, cerebrospinal fluid volume, cerebral white matter high signal volume, and regional gray and cerebrospinal fluid volumes. SBM was used to derive morphological indicators such as cortical thickness, curvature, and sulcal depth. Quantitative calculations of DWI images were performed using FMRIB's Software Library[9] to generate ADC images for each participant. Based on the Brainnetome Atlas[10], mean values of all quantitative metrics were extracted for each brain region. By comparing these indicators between the alcohol group and the non-alcohol group, the study assessed the correlation between these metrics and the degree of alcohol consumption and the morphological characteristics of distal intracranial arteries.

Research has established that alcohol abuse heightens the risk of cerebrovascular events by altering cerebral blood flow, increasing blood pressure, and compromising the blood–brain barrier. Short-term alcohol consumption significantly enlarges the perivascular space surrounding small vessels in brain tissue, whereas long-

term consumption induces pathological changes in the basilar arteries (BAs), such as endothelial detachment, fragmentation of the internal elastic lamina (IEL), and thickening of the peritubular middle and outer layers[11]. Significant correlations have been identified between cerebral blood flow and structural parameters across various brain regions, including the temporal, frontal, parietal, and occipital lobes, precentral gyrus, periaqueductal cortex, internal olfactory cortex, supramarginal gyrus, fusiform gyrus, precuneus, and pallidum in patients with cognitive dysfunction[12]. Additionally, a marked correlation exists between reduced cerebral blood flow and gray matter atrophy, affecting cortical volume, surface area, and thickness across numerous regions[12]. Gould et al. demonstrated that vascular characteristics of distal arteries on 3D-TOF MRA, such as vessel length and branching patterns, can serve as surrogate markers of cerebral blood flow. Morphological features of distal intracranial arteries—including arterial length, density, and mean tortuosity—measured by 3D-TOF MRA, were found to correlate with systemic or focal atrophy in cerebral small vessel disease[13]. 3D-TOF MRA remains the most commonly employed angiographic technique in clinical practice, particularly for evaluating the head and carotid arteries[14]. Advances in image processing techniques have facilitated the extraction of cerebrovascular features using 3D-TOF MRA[15–18].

The primary subjects of this study are individuals characterized by a long-standing pattern of alcohol consumption behavior, as opposed to those who have already manifested alcohol use disorders. This study quantified the morphological characteristics of distal intracranial arteries, including mean arterial density, radius, length, curvature, flexibility, and tortuosity, by processing MRA images with MIMICS and 3D Slicer[19,20]. Differences in these metrics between the alcohol group and the non-alcohol group were analyzed, alongside their relationships with various brain structures, such as gray matter volume (GMV), white matter volume (WMV), cerebrospinal fluid volume (CSFV), cerebral white matter high signal volume (WMH). Previous studies mainly focused on either brain structural changes or vascular alterations in chronic alcoholics separately.

Our study innovatively combines vascular morphological data, such as mean arterial density, radius and length, with standard neuroimaging metrics like GMV, WMV, CSFV and WMH. This integrated approach allows for a more comprehensive understanding of the complex relationship between chronic alcohol consumption, cerebrovascular changes, and brain structural remodeling, filling a gap in the existing literature.

The primary research question of this study is: By quantitatively assessing the morphological characteristics of distal intracranial arteries, including parameters such as density, radius, and length, to investigate how these characteristics of distal intracranial vessels change in long-term alcoholics and study the relationship between them and structural brain alterations. We hypothesize that there is a significant association between cerebrovascular morphological changes and structural brain modifications in long-term alcoholics. In particular, changes in arterial density, radius, and length are expected to be related to changes in gray matter volume (GMV), white matter volume (WMV), and cerebrospinal fluid volume (CSFV). It is anticipated that these vascular changes will contribute to the overall structural brain changes resulting from long-term alcohol consumption.

Materials and methods

Participants

From December 2022 to December 2023, a total of 71 participants with chronic alcohol consumption and 82 participants in the control group with no history of alcohol consumption were consecutively recruited from neurology inpatients and outpatient services.

In the chronic alcohol consumption group, Twenty-one cases were excluded. Nineteen cases did not complete the nuclear magnetic examination as required. Two cases had MRI scans with significant motion artifacts.

In the control group without alcohol consumption history, Thirty-nine cases were excluded. Fourteen cases did not complete the required nuclear magnetic examination. Twelve cases had acute cerebral infarction after examination. Six cases had intracranial aortic stenosis after examination. Seven cases had a clear white matter lesion.

Eventually, a total of 50 chronic alcoholics and 43 non-alcoholics were recruited.

Long-term Alcohol Consumption Group.

Inclusion criteria: (1) Complete medical records; (2) Age 22 to 65 years; (3) Right-handed; (4) Males with an alcohol intake exceeding 40 g (degree × mL) per day or more than 280 g per week, and females with an alcohol intake exceeding 20 g (degree × mL) per day or more than 140 g per week, with a history of alcohol consumption spanning more than 5 years[21,22]; (5) Informed about the study and provided voluntary participation.

Exclusion criteria: (1) Neurological damage due to other diseases; (2) History of traumatic brain injury or other brain tissue damage; (3) Use of psychotropic drugs in the last 3 months; (4) Drug dependence or other substance abuse; (5) Cognitive dysfunction; (6) Epilepsy; (7) Contraindications to MRI examination.

The participants of our study are from Jincheng City, Shanxi Province, where females basically do not consume alcohol. All the enrolled participants were male, with ages ranging from 22 to 65 years.

Classification of alcohol consumption groups (based on weekly alcohol intake × years of consumption): Light drinking group: 4000–10000 g; Moderate drinking group: 10001–20000 g; Heavy drinking group: More than 20000 g[23].

Inclusion criteria for the no alcohol consumption group: (1) Age and gender matched, no history of continuous alcohol consumption; (2) Complete medical history with no serious neurological or psychiatric diseases; (3) Right-handed; (4) No history of traumatic brain injury or other brain tissue damage; (5) No recent use of psychotropic medications; (6) Informed about the study content and provided voluntary participation.

This study was approved by the Ethics Committee of Jincheng City People's Hospital (JCPH.NO20230710004). All participants, or their guardians, provided written informed consent.

Data collection

Demographic data

Information was recorded on participants' age, gender, body mass index (BMI), hypertension, diabetes mellitus, coronary atherosclerotic heart disease, smoking history, and previous incidents of cerebral infarction or cerebral hemorrhage.

Collection of general metabolic markers

The general metabolic indices were derived from the laboratory of Jincheng People's Hospital. The subjects provided fresh blood samples through venous blood collection, which were then collected into inert separator gel procoagulant tubes. The collected venous blood was centrifuged at 2000 rpm for 20 min at 4 °C as rapidly as possible. Subsequently, the supernatant was aspirated using a pipette gun to obtain serum.

Leukocytes, erythrocytes, hemoglobin, hematocrit, MCV, MCH, MCHC, platelets, plateletcrit, absolute lymphocyte count, lymphocyte percentage, absolute monocyte count, monocyte percentage, absolute neutrophil count, neutrophil percentage, absolute eosinophil count, eosinophil percentage, absolute basophil count, basophil percentage, nucleated red blood cell count, nucleated red blood cell percentage and large platelet percentage were measured using an automated hematology analyzer. Biochemical markers such as calcium, carbon dioxide, phosphorus, magnesium, ALT, AST, total bilirubin, urea, creatinine, cholinesterase, alkaline phosphatase, gamma-glutamyl transferase, lactate dehydrogenase, adenosine deaminase and uric acid were determined by enzymatic methods on a biochemical analyzer. For lipid markers such as total cholesterol, triglycerides, and high-density lipoprotein cholesterol (HDL-C), enzymatic colorimetric assays were employed. Glycated Hemoglobin was measured using the high-performance liquid chromatography (HPLC) method. Homocysteine levels were determined using the enzymatic cycling method. Prothrombin time (PT), fibrinogen (FIB), thrombin time (TT), and activated partial thromboplastin time (APTT) were measured using the coagulation method. D-dimer levels were measured via the immunoturbidimetric method. Serum myoglobin, CK–MB mass, FT3, FT4, TSH, folate, vitamin B12, and ferritin levels were measured using the electrochemiluminescence immunoassay method.

Cognitive and psychometric assessments

Participants were evaluated using the AUDIT scale[24], Alcohol Dependence Self-Rating Scale, PSQI Sleep Scale, MMSE, MoCA, and Symptom Checklist 90 (SCL-90).

Blood sample collection and processing

Fresh blood samples were obtained via venipuncture and collected into inert separator gel procoagulant tubes. The samples were centrifuged at 4 °C for 20 min at 2000 rpm, and the supernatant was carefully extracted using a pipette, then stored in 1.5 ml polypropylene tubes at − 80 °C until analysis. The following markers were measured: IL-1b, complement C1q, IL-2, IL-4, IL-6, IL-10, TNF-α, INF-γ, GFAP, and sTREM2.

MRI imaging and image processing

All participants underwent MRI using a standard protocol. Scanning was performed with a 3.0 T Philips Intera scanner (Ingenia 3.0 T, Philips Medical Systems, The Netherlands) in the imaging department of Jincheng People's Hospital. The imaging consists of the following sequences: DWI (repetition time (TR) = 3240 ms, echo time (TE) = 113 ms, flip angle (FA) = 90°, slice = 20, field of view (FOV) = 230 × 230mm^2, acquisition matrix = 164 × 134, thickness = 5.5 mm, voxel size = 1.4 × 1.7 × 5.5 mm^3), T1-weighted (repetition time (TR) = 1800 ms, echo time (TE) = 20 ms, flip angle (FA) = 90°, slice = 20, field of view (FOV) = 230 × 185 mm^2, acquisition matrix = 322 × 134, thickness = 5.5 mm, voxel size = 1.4 × 1.7 × 5.5 mm^3), T2-weighted (TR = 4,000 ms, TE = 107 ms, FA = 90°, slice = 20, FOV = 230 × 230 mm^2, acquisition matrix = 384 × 384, thickness = 5.5 mm, voxel size = 0.6 × 0.7 × 5.5 mm^3), FLAIR (TR = 11,000 ms, TE = 120 ms, FA = 90°, slices = 20, FOV = 230 × 187mm^2, acquisition matrix = 356 × 115, thickness = 5.5 mm, voxel size = 0.65 × 1 × 5.5mm^3), TOF-MRA (TR = 23 ms, TE = 3.5 ms, FA = 18°, slice = 160, FOV = 200 × 200 mm^2, acquisition matrix = 444 × 294, thickness = 1.2 mm, voxel size = 0.45 × 0.68 × 1.2 mm^3), 3D-T1 (TR = 7.9 ms, TE = 3.5 ms, FA = 8°, slice = 360, FOV = 256 × 256 mm^2, acquisition matrix = 256 × 256, thickness = 1 mm, voxel size = 1 × 1 × 1 mm^3).

Based on Matlab 2020, data preprocessing and statistical analysis of brain structure images were carried out using the CAT12 software package. The specific procedures are as follows:

① Data Conversion: Convert the DICOM data collected by the device into the analyzable NIFTI format. ② Data Inspection: Check the imaging quality of the data one by one, mainly focusing on the integrity of data collection and whether there are serious artifacts. ③ Brain Structure Image Segmentation: Utilize CAT12 to segment the images into gray matter, white matter, and cerebrospinal fluid, and perform modulation to enable volume analysis. ④ Cortical Segmentation: Employ CAT12 for cortical segmentation, and estimate the thickness, curvature, and sulcal depth of the cortical regions. ⑤ Quantitative Calculation: Extract the total intracranial volume (TIV), as well as the volumes of gray matter and white matter in each brain region, and store them in a table. ⑥ Region-of-Interest Extraction: Use the HCP-MMP1[25]atlas to extract the average thickness, curvature, and sulcal depth of each cortical region. Use the Neuromorphometrics atlas to extract the average volume information of gray matter and white matter in each region. ⑦ Gaussian Smoothing of Brain Structure Images: Apply Gaussian smoothing to the segmented images with a Gaussian kernel having a full-width at half-maximum of 12 mm^3. ⑧ Voxel-Based Morphometry (VBM) Pixel-by-Pixel Statistical Analysis: Based on the general linear model, establish a statistical analysis model for the smoothed brain structure data and conduct pixel-by-pixel statistical analysis. ⑨ Surface-Based Morphometry (SBM) Statistical Analysis: Based on the general linear model, establish a statistical analysis model for the smoothed cortical quantitative information and carry out pixel-by-pixel statistical analysis.

Preprocessing and quantitative calculations of DWI images were conducted using FMRIB's Software Library (FSL). ① Data Conversion: Convert the DICOM data collected by the device into the analyzable NIFTI format. ② Data Inspection: Check the imaging quality of the data one by one, mainly focusing on the integrity of data collection and whether there are serious artifacts. ③ Quantitative Calculation: Use FSL to perform quantitative calculations on DWI images to obtain the ADC image for each patient. ④ Spatial Alignment: Taking each subject's T1 image as a reference, perform a 6-parameter rigid body transformation to spatially align the ADC image with the T1 image. ⑤ Spatial Normalization: Since the shape and size of each subject's brain differ, in order to conduct voxel-by-voxel statistical analysis on one or more groups of data, all subjects need to be aligned voxel by voxel first. Using the T1-weighted brain template in MNI space as the reference standard, estimate the registration parameters with the T1 image as the source image. Then, perform a 12-parameter affine transformation and non-linear deformation on the ADC index image for spatial transformation, normalizing the quantitative index brain images of all subjects to the template space to eliminate inter-subject differences. ⑥ Gaussian Smoothing: Apply Gaussian smoothing to the spatially normalized data with a Gaussian kernel having a full-width at half-maximum of 8 mm^3 to further remove noise and make the data for statistical analysis conform to a normal distribution. ⑦ Quantitative Index Extraction: Based on the BrainnetomeAtlas atlas, extract the average value of all quantitative indices in each brain region and store it in an Excel spreadsheet. ⑧ Pixel-by-Pixel Statistical Analysis: Based on the general linear model, establish a statistical analysis model for the smoothed ADC data and conduct pixel-by-pixel statistical analysis.

All MRA images were processed using MIMICS and 3D Slicer. Initially, the medical images were meticulously examined one by one to ensure their completeness and quality. Subsequently, the 3D VR function of RadiAnt DICOM Viewer 2023.1 (Medixant, Poznan, Poland) was utilized to segment the DICOM images into blood vessels, bones, and other tissues. Through this process, patient-specific cerebral artery models were reconstructed. By carefully adjusting the display threshold, the visibility of non-cerebral artery parts was significantly reduced. In the next step, the adjusted models were imported into Mimics Research 19.0 (Materialise, Leuven, Belgium), and the Edit Mask function was employed to further refine the models, precisely retaining only the regions of interest. Finally, in 3D Slicer (Harvard Medical School, Boston, MA, USA), the centerlines of the cropped models were computed. This enabled the extraction of average morphological parameters, such as radius, curvature, and tortuosity, for various regions in each case. Additionally, the 3D models were converted into volumes for volumetric analysis. The vascular centerlines were obtained using 3D Slicer software. Subsequently, the perpendicular distances from each point on the centerline to the straight line connecting the starting and ending points were calculated. The sum of the squares of these distances was normalized to obtain the arterial tortuosity index. Regarding arterial flexibility, we employed a method based on the centerline deviation method. The flexibility was evaluated according to the curvature changes of the vascular centerlines. Moreover, to minimize the impact of head movement and vascular pulsation on the measurement results, during the scanning process, we requested patients to remain stationary. Additionally, electrocardiogram-gated (ECG-gated) technology was used to synchronously collect data, ensuring image acquisition during the relatively stable phases of vascular pulsation. The geometric information of all cases was collated and stored in Excel 2016 (Microsoft, Redmond, WA, USA) for subsequent statistical analysis. To validate the accuracy of the automated extraction of vascular features, we assigned two experienced radiologists to independently conduct a manual review of the vascular segmentation results and feature extraction. The radiologists carefully examined each vascular model, comparing the automated segmentation results with the actual vascular morphology. They manually corrected any parts with segmentation errors or inaccuracies. In addition, we carried out both intra-rater and inter-rater reliability evaluations. In the intra-rater reliability evaluation, a single researcher performed two vascular measurements on the identical samples at separate time points. The Intraclass Correlation Coefficient (ICC) was then calculated based on these two sets of measurement results to assess the consistency within the same rater. For the inter-rater reliability evaluation, two distinct researchers measured the same samples. The ICC of their measurement outcomes was determined to evaluate the agreement between different raters. By conducting these evaluations, we are able to efficiently validate the consistency of arterial measurement data and guarantee the reliability of our research results. Mean vessel density was calculated as the ratio of vessel volume to total intracranial volume. The extracted intracranial artery group included segments M2, M3, and M4 of the MCA, segments A2, A3, and A4 of the ACA, and segments P2, P3, and P4 of the PCA.

Statistical analysis

Continuous variables conforming to a normal distribution were presented as the mean ± standard deviation (SD), whereas those with a non-normal distribution were reported as the median (interquartile range). Categorical variables were expressed as frequencies (percentages). The Shapiro–Wilk test was utilized to assess the normality of continuous variables.

Differences in normally distributed continuous data between two groups were analyzed using Student's t-test, while comparisons among multiple groups were performed using one-way ANOVA. For continuous data that did not follow a normal distribution, the Wilcoxon test was used for two-group comparisons, and the Kruskal–Wallis rank sum test was employed for multiple-group comparisons. Differences in categorical data between groups were assessed using the chi-square test.

When comparing gray matter volume (GMV), white matter volume (WMV), cerebrospinal fluid volume (CSFV), and white matter hyperintensity volume (WMH) across different alcohol-consuming groups, multiple testing was necessary. Bonferroni correction was applied for multiple-comparison adjustment to ensure result validity and reliability.

Multiple-comparison corrections were carried out in:

Comparing ADC values, GMV, CSFV, cortical thickness, curvature, and sulcal depth between the alcohol-consuming and control groups.

Examining the associations between alcohol consumption levels and ADC values, GMV, CSFV, cortical thickness, curvature, and sulcal depth in relevant brain regions within the alcohol-consuming group.

In these multiple-comparison analyses, adjusted p-values from Bonferroni correction were used, with adjusted $p < 0.05$ indicating statistical significance.

Control variables including age, previous cerebral infarction history, previous cerebral hemorrhage history, hypertension, diabetes mellitus, coronary atherosclerotic heart disease, and smoking status were included in correlation analyses between alcohol consumption levels and ADC values, GMV, CSFV, cortical thickness, curvature and sulcal depth.

To account for brain size effects, distal artery length, radius, curvature, flexibility, and tortuosity were normalized by taking the cube root of total intracranial volume (TIV). GMV, WMV, CSFV, WMH, regional gray matter and cerebrospinal fluid volumes were also normalized using TIV. In each brain region, cortical thickness, sulcal depth, and tortuosity were normalized relative to TIV.

For statistical analyses without multiple-group comparisons, uncorrected p-values were reported, with $p < 0.05$ for significance. All analyses were conducted using SPSS 26.0 (IBM, Armonk, NY, USA), and correlation coefficients were visualized as a matrix in Origin2024b.

Results

Baseline characteristics

A total of 50 alcoholics and 43 non-alcoholics, aged 22–65 years, were enrolled in the study. MR imaging was successfully completed for all participants. Clinical data were collected upon admission, and laboratory data were obtained within 24 h of admission.

Among the general metabolic indices, significant differences were observed in MCH, MCHC, platelets, platelet pressure product, total bilirubin, alkaline phosphatase, glutamyltransferase, triglycerides, ferritin, MMSE score, and MoCA score.

Specifically, the levels of MCH, MCHC, total bilirubin, glutamyltransferase, triglycerides, and ferritin were higher in alcoholics. In contrast, the levels of platelets, platelet pressure product, alkaline phosphatase, as well as MMSE and MoCA score were lower in alcoholics compared to the non-alcoholics. The data are presented in Table 1.

Baseline characteristics	Alcohol consumption (n = 71)	No alcohol consumption (n = 82)	*P*	X^2
Basic characteristic				
Age(years)	55 (47.75, 60.25)	53 (46, 58)	0.072	
BMI	25.6 ± 0.58	24.7 ± 0.41	0.224	
Male(%)	50 (100%)	43 (100%)		
Previous cerebral infarction (%)	22 (44%)	20 (46.5%)	0.576	0.000
Previous cerebral hemorrhage (%)	2 (4%)	0	0.286	1.758
Hypertension (%)	34 (68%)	20 (46.5%)	0.069	2.868
Diabetes (%)	6 (12%)	3 (7%)	0.324	0.667
Coronary heart disease (%)	3 (6%)	3 (7%)	0.587	0.037
Smoking history(%)	27 (54%)	20 (46.5%)	0.304	0.519
General metabolic indicators				
MCH, pg	31.8 (30.6, 33.05)	31.4 (30.1, 32.4)	0.014	
MCHC, g/L	347.00 (340.50, 354.50)	343.00 (339.00, 350.00)	0.007	
Platelet, 10^9/L	223.28 ± 54.746	247.81 ± 59.044	0.002	
Platelet blood pressure, %	220.00 (190.00, 262.50)	249.00 (214.00, 290.00)	0.011	
Total bilirubin, μmol/L	14.500 (11.400, 18.825)	12.300 (9.500, 17.500)	0.034	
Alkaline phosphatase, U/L	66.926 ± 20.4708	80.781 ± 20.1774	0.000	
Glutamyl transferase, U/L	32.500 (20.750, 62.000)	23.000 (17.075, 31.000)	0.001	
Triglyceride, mmol/L	1.7000 (1.2775, 2.4225)	1.4800 (1.0300, 1.9600)	0.012	
Ferritin, ng/mL	143.70 (92.15, 289.95)	121.00 (67.60, 187.50)	0.020	
Meters				
MMSE	29.00 (25.00, 30.00)	30.00 (29.25, 30.00)	0.001	
MoCA	27.00 (21.00, 30.00)	30.00 (30.00, 30.00)	0.000	

Table 1. Baseline characteristics. For data following a normal distribution, they are presented as mean ± standard deviation. Data with non-normal distribution are presented as median (interquartile range). Categorical variables are presented as number (percentage). Differences in normally distributed continuous data between two groups were analyzed using Student's t-test. For continuous data that did not follow a normal distribution, the Wilcoxon test was used for two-group comparisons. Differences in categorical data between groups were assessed using the chi-square test. The *P* values were not adjusted for multiple testing.

Baseline characteristics	Alcohol consumption (n = 50)	No alcohol consumption (n = 43)	*P*
Cytokine			
IL-1B, pg/mL	88.285 (76.523, 94.576)	103.661 (90.746, 124.687)	0.000
IL-2, pg/mL	0.490 (0.420, 0.555)	0 .490 (0.470, 0.560)	0.281
IL-4, pg/mL	0.6250 (0.5500, 0.7100)	0 .6100 (0.5400, 0.7175)	0.326
IL-6, pg/mL	3.4400 (2.5050, 8.5325)	2.6750 (2.0125, 4.0300)	0.016
IL-10, pg/mL	0.8600 (0.7300, 1.1100)	0.7400 (0.6450, 0.9425)	0.013
INF-r, pg/mL	0.8800 (0.5775, 2.2625)	0.7500 (0.5250, 2.2000)	0.413
TNF-α, pg/mL	0.8400 (0.7025, 1.0575)	0.8700 (0.7275, 1.0125)	0.427
Complement-c1q, ng/mL	19.0746 (17.4890, 21.3856)	18.8012 (16.9530, 21.6891)	0.459
Neuroinflammatory markers			
GFAP, pg/mL	2.8304 (2.1252, 3.3731)	3.5179 (2.2160, 4.6289)	0.044
sTREM2, pg/mL	8.1485 (6.4560, 10.9825)	9.1600 (7.9750, 13.8800)	0.045

Table 2. Baseline characteristics. Data with non-normal distribution are presented as median (interquartile range). The Wilcoxon test was used for two-group comparisons. The *P* values were not adjusted for multiple testing.

	Alcohol consumption (n = 50)	No alcohol consumption (n = 43)	*P*
GMV (%)	0.40140656 ± 0.028659986	0.42184650 ± 0.025499295	0.001
WMV (%)	0.35761594 (0.32366904, 0.37074059)	0.36787292 (0.35323437, 0.37520388)	0.007
CSFV (%)	0.24435050 ± 0.047034314	0.20903606 ± 0.041906371	0.000
WMH (%)	0.00159949 (0.00078879, 0.00527485)	0.00088116 (0.00063316, 0.00132647)	0.006
Mean arterial density (%)	0.76925614 ± 0.138366234	0.87553934 ± 0.204801143	0.004
Mean arterial radius (%)	0.10305433 ± 0.006918745	0.10717321 ± 0.10717321	0.007
Mean arterial length (%)	4.67323115 ± 0.483342522	4.71445164 ± 0.518264427	0.694
Mean arterial curvature (%)	0.01268054 ± 0.001456298	0.01232036 ± 0.001223155	0.206
Mean arterial flexibility (%)	− 0.00023101 (− 0.00434450, 0.00355777)	− 0.00309746 (− 0.00762306, 0.00192313)	0.048
Mean arterial tortuosity (%)	0.03024906 (0.02430322, 0.03768975)	0.03321715 (0.02724495, 0.04222822)	0.015

Table 3. Statistical analysis of gray matter volume, white matter volume, cerebrospinal fluid volume, high signal volume of cerebral white matter and morphological characteristics of distal intracranial arteries in alcohol consumption and no alcohol consumption groups. Data conforming to a normal distribution are presented as mean ± standard deviation, while data with a non-normal distribution are presented as median (interquartile range). For normally distributed continuous data, differences between two groups were analyzed using Student's t-test. As for non-normally distributed data between two groups, the Wilcoxon test was employed for the comparison. The P values were not adjusted for multiple testing.

Regarding cytokines and neuroinflammatory markers, significant differences were found in IL-1b, IL-6, IL-10, GFAP, and sTREM2. IL-1b, GFAP, and sTREM2 levels were lower in alcoholics, whereas IL-6 and IL-10 levels were higher. The data are presented in Table 2.

Brain structures and vascular differences between alcoholics and non-alcoholics

Significant differences were observed in gray matter volume, white matter volume, cerebrospinal fluid volume, and cerebrospinal fluid high signal volume between alcoholics and non-alcoholics. Alcoholics exhibited lower gray matter and white matter volumes, while cerebrospinal fluid volume and cerebral white matter high signal volume were higher. These data are presented in Table 3.

Significant differences were also found in mean arterial density, mean arterial radius, mean arterial flexibility, and mean arterial tortuosity between the two groups. Alcoholics had lower mean arterial density, mean arterial radius, and mean arterial tortuosity, while mean arterial flexibility was higher. These data are presented in Table 3.

Additionally, with increasing alcohol consumption, there was a progressive decrease in gray matter and white matter volumes, accompanied by a gradual increase in cerebrospinal fluid volume and cerebral white matter high signal volume. These data are presented in Table 4.

Correlation analysis

Alcohol consumption was negatively correlated with gray matter volume ($P < 0.05$)and white matter volume ($P < 0.05$) and positively correlated with cerebrospinal fluid volume ($P < 0.05$) and cerebral white matter high signal volume ($P < 0.05$). Notably, alcohol consumption was negatively correlated with mean arterial density ($P < 0.05$), mean arterial radius ($P = 0.051$), and mean arterial length ($P < 0.05$), with significant correlations

	Mild alcoholics	Moderate alcoholics	Heavy alcoholics	adjusted_p
GMV(%)	0.41260851 ± 0.02174240	0.39975940 ± 0.019090326	0.37206723 ± 0.025484583	0.002
WMV(%)	0.36266887 (0.35031318, 0.37078838)	0.35478620 (0.33407305, 0.37703570)	0.32220041 (0.31059223, 0.33844736)	0.016
CSFV(%)	0.22742135 ± 0.040645031	0.24279666 ± 0.033874961	0.29409972 ± 0.042399624	0.002
WMH (%)	0.00109096 (0.00066056, 0.00227229)	0.00208457 (0.00082763, 0.00667493)	0.00596124 (0.00221042, 0.00999109)	0.013

Table 4. Statistical analysis of gray matter volume, white matter volume, cerebrospinal fluid volume, and cerebral white matter high signal volume in groups with different levels of alcohol consumption. Data conforming to a normal distribution are presented as mean ± standard deviation, while data with a non-normal distribution are presented as median (interquartile range). For normally distributed continuous data, differences between two groups were analyzed using Student's t-test. As for non-normally distributed data between two groups, the Wilcoxon test was employed for the comparison. The *P*-values were corrected using the Bonferroni method.

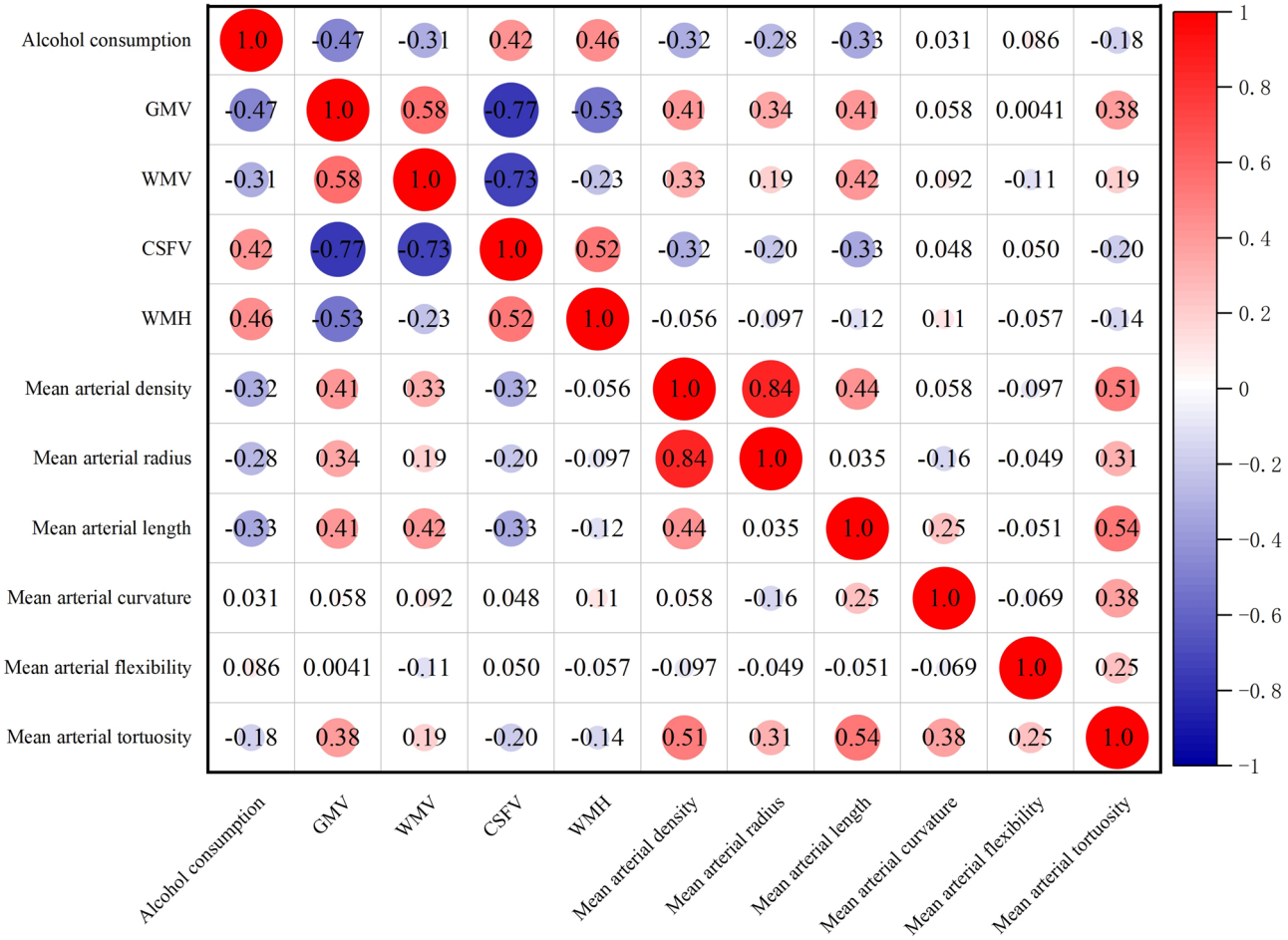

Fig. 1. Correlation analysis of alcohol consumption, gray matter volume, white matter volume, cerebrospinal fluid volume, cerebral white matter high signal volume, and morphological characteristics of distal intracranial arteries. The numerical values within the matrix denote correlation coefficients.

observed for mean arterial density and mean arterial length. The correlations with mean arterial curvature ($P = 0.83$), mean arterial flexibility ($P = 0.56$), and mean arterial tortuosity ($P = 0.22$) were not significant.

Furthermore, in alcoholics, gray matter volume was positively correlated with mean arterial density ($P < 0.05$), mean arterial radius ($P < 0.05$), mean arterial length ($P < 0.05$), and mean arterial tortuosity ($P < 0.05$), with significant correlations. White matter volume showed a significant positive correlation with mean arterial density ($P < 0.05$) and mean arterial length ($P < 0.05$). Conversely, cerebrospinal fluid volume was negatively correlated with mean arterial density ($P < 0.05$) and mean arterial length ($P < 0.05$), with significant correlations. These relationships are illustrated in Fig. 1.

Comparison of alcoholics and non-alcoholics

ADC values across all brain regions were higher in alcoholics compared to non-alcoholics. Using the Brainnetome Atlas to segment the brain into 246 regions, ADC values were observed with statistically significant differences in 134 of these regions. The corresponding brain regions with significant correlations are detailed in Table 5.

Additionally, the brain regions that showed significant differences in gray matter volume mainly included the following areas: Left Hippocampus, Left Basal Forebrain, Left Middle Occipital Gyrus, Right Amygdala, Right Basal Forebrain, Right Inferior Occipital Gyrus, Right Middle Occipital Gyrus and Right Posterior Orbital Gyrus. These data are presented in Table 6.

Moreover, the brain regions exhibiting significant differences in cerebrospinal fluid volume mainly encompass the following areas: Left Cerebrospinal Fluid (Left CSF) region, Left Hippocampus, Left Angular Gyrus, Left Central Operculum, Left Inferior Temporal Gyrus, Left Subcallosal Area, Right Cerebrospinal Fluid (Right CSF) region, Right Calcarine Cortex and Right Cuneus. These data are presented in Table 6.

Cortical thickness, sulcal depth, and curvature were classified according to HCP-MMP1 mapping. The statistically significant differences in cortical thickness were tabulated in Table 7. Specifically, four brain regions demonstrated significance in cortical thickness: Left Area anterior 9-46v, Left Area_TA2, Left Medial Belt Complex, and Right Pirform_Cortex. In contrast, after multiple-test correction, no significant differences in sulcal depth and curvature were detected across any of the brain regions between the two groups. In regions where differences were statistically significant, alcoholics exhibited lower cortical thickness.

In addition to these results, a correlation analysis was conducted to explore the relationships between alcohol consumption levels and apparent diffusion coefficient (ADC) values, gray matter volume (GMV), cerebrospinal fluid volume (CSFV), cortical thickness, curvature, and sulcal depth in relevant brain regions among individuals in the alcohol-consuming group. Variables such as age, history of previous cerebral infarction, history of previous cerebral hemorrhage, hypertension, diabetes, coronary heart disease, and smoking history were taken into account as potential confounding factors.

Correlation of ADC values in alcoholics

In individuals with alcoholism, the apparent diffusion coefficient (ADC) values were positively correlated with the quantity of alcohol consumed. Before accounting for confounding factors, 50 brain regions exhibited significant correlations. The specific brain regions with significant correlations are presented in Table 8. After controlling for confounding factors, the ADC values in 45 brain regions remained associated with the amount of alcohol consumed. The detailed information can be found in Table 9.

Correlation of gray matter volume in alcoholics

Prior to controlling for confounding factors, the gray matter volume in 11 brain regions was correlated with the amount of alcohol consumed. These regions were the Left 4th Ventricle, Left Amygdala, Left Brainstem, Left Cerebellum White Matter, Left Hippocampus, Left Entorhinal Area, Right 4th Ventricle, Right Brainstem, Right Entorhinal Area, Right Fusiform Gyrus, and Right Gyrus Rectus.

Among these regions, the gray matter volumes of the Left 4th Ventricle, Left Brainstem, Left Cerebellum White Matter, Right 4th Ventricle, and Right Brainstem showed a positive correlation with the amount of alcohol consumed. In contrast, the gray matter volumes of the remaining regions were negatively correlated with the amount of alcohol consumed. The detailed information is presented in Table 10.

After controlling for confounding factors, it was found that the gray matter volumes in 5 brain regions were correlated with the amount of alcohol consumed. These regions included the Right Accumbens, Left Hippocampus, Left Posterior Insula, Right Posterior Orbital Gyrus, and Left Planum Polare. Furthermore, the gray matter volumes in all of these regions showed a positive correlation with the amount of alcohol consumed. The detailed data can be found in Table 11.

Correlation of cerebrospinal fluid volume in alcoholics

Prior to controlling for confounding factors, the cerebrospinal fluid volume in 10 brain regions was correlated with the amount of alcohol consumed. These regions were the Left Caudate, Left Hippocampus, Left Thalamus Proper, Left Inferior Temporal Gyrus, Left Middle Cingulate Gyrus, Left Posterior Insula, Left Planum Polare, Right Accumbens, Right Lateral Orbital Gyrus, and Right Posterior Orbital Gyrus. All of these brain regions exhibited a positive correlation between their cerebrospinal fluid volumes and the amount of alcohol consumed. The detailed information can be found in Table 12.

After accounting for confounding factors, the cerebrospinal fluid volume in 5 brain regions was found to be correlated with the amount of alcohol consumed. These regions were the Right Accumbens, Left Hippocampus, Left Posterior Insula, Right Posterior Orbital Gyrus, and Left Planum Polare. Moreover, the CSFV in all of these regions showed a positive correlation with the amount of alcohol consumed. The detailed data are presented in Table 13.

Correlation of cortical thickness in alcoholics

After controlling for confounding factors, the cortical thickness in 13 brain regions was found to be correlated with the amount of alcohol consumed. These brain regions encompassed Area_3a, Area_43, Area_52, Posterior Insular Area 2, Area_TA2, Frontal Opercular_Area 1, Area_Posterior Insular_1, Medial Belt Complex, and Para-Insular_Area on the left hemisphere, and Area_3a, Area_52, Area_TA2, and Para-Insular_Area on the right hemisphere. The cortical thickness in all of these brain regions exhibited a negative correlation with the amount of alcohol consumed. The detailed information can be found in Table 14.

Hemisphere	Region	adjusted_p	Hemisphere	Region	adjusted_p
Left	dorsolateral area 8	0.000	Right	dorsolateral area 8	0.000
	lateral area 9	0.000		dorsal area 9/46	0.000
	dorsal area 9/46	0.000		inferior frontal junction	0.000
	inferior frontal junction	0.000		area 46	0.000
	area 46	0.000		ventral area 9/46	0.000
	ventrolateral area 8	0.000		ventrolateral area 8	0.000
	ventrolateral area 6	0.000		ventrolateral area 6	0.000
	opercular area 44	0.000		lateral area10	0.000
	medial area 14	0.000		inferior frontal sulcus	0.000
	area 13	0.000		opercular area 44	0.000
	area 4(head and face region)	0.000		medial area 14	0.000
	area 4(tongue and larynx region)	0.000		lateral area 11	0.000
	area 41/42	0.000		area 13	0.000
	TE1.0 and TE1.2	0.000		lateral area 12/47	0.000
	caudal area 22	0.000		area 4(head and face region)	0.000
	dorsolateral area37	0.000		caudal dorsolateral area 6	0.000
	anterior superior temporal sulcus	0.000		area 4(tongue and larynx region)	0.000
	intermediate lateral area 20	0.000		caudal ventrolateral area 6	0.000
	rostroventral area 20	0.000		area 41/42	0.000
	medioventral area37	0.000		TE1.0 and TE1.2	0.000
	lateroventral area37	0.000		caudal area 22	0.000
	caudal area 35/36	0.000		lateral area 38	0.000
	posterior parahippocampal gyrus	0.000		rostral area 22	0.000
	entorhinal cortex	0.000		anterior superior temporal sulcus	0.000
	rostroposterior superior temporal sulcus	0.000		rostroventral area 20	0.000
	caudoposterior superior temporal sulcus	0.000		medioventral area37	0.000
	rostral area 7	0.000		lateroventral area37	0.000
	caudal area 7	0.000		rostral area 35/36	0.000
	lateral area 5	0.000		caudal area 35/36	0.000
	postcentral area 7	0.000		posterior parahippocampal gyrus	0.000
	intraparietal area 7(hIP3)	0.000		entorhinal cortex	0.000
	rostrodorsal area 39(Hip3)	0.000		rostroposterior superior temporal sulcus	0.000
	rostrodorsal area 40(PFt)	0.000		caudoposterior superior temporal sulcus	0.000
	caudal area 40(PFm)	0.000		rostral area 7	0.000
	rostroventral area 39(PGa)	0.000		caudal area 7	0.000
	rostroventral area 40(PFop)	0.000		lateral area 5	0.000
	dorsomedial parietooccipital sulcus(PEr)	0.000		postcentral area 7	0.000
	head and face region	0.000		intraparietal area 7(hIP3)	0.000
	area 1/2/3(tongue and larynx region)	0.000		rostrodorsal area 39(Hip3)	0.000
	area 2	0.000		rostrodorsal area 40(PFt)	0.000
	hypergranular insula	0.000		caudal area 40(PFm)	0.000
	ventral agranular insula	0.000		rostroventral area 39(PGa)	0.000
	dorsal agranular insula	0.000		rostroventral area 40(PFop)	0.000
	ventral dysgranular and granular insula	0.000		medial area 7(PEp)	0.000
	dorsal granular insula	0.000		dorsomedial parietooccipital sulcus(PEr)	0.000
	dorsal dysgranular insula	0.000		head and face region	0.000
	dorsal area 23	0.000		area 1/2/3(tongue and larynx region)	0.000
	subgenual area 32	0.000		area 2	0.000
	rostral cuneus gyrus	0.000		hypergranular insula	0.000
	rostral lingual gyrus	0.000		ventral agranular insula	0.000
	ventromedial parietooccipital sulcus	0.000		dorsal agranular insula	0.000
	area V5/MT +	0.000		ventral dysgranular and granular insula	0.000
	lateral superior occipital gyrus	0.000		dorsal granular insula	0.000
	rostral hippocampus	0.000		dorsal dysgranular insula	0.000
	caudal hippocampus	0.000		dorsal area 23	0.000
	dorsolateral putamen	0.000		rostroventral area 24	0.000

Continued

Hemisphere	Region	adjusted_p	Hemisphere	Region	adjusted_p
	medial pre-frontal thalamus	0.000		subgenual area 32	0.000
	sensory thalamus	0.000		rostral cuneus gyrus	0.000
	rostral temporal thalamus	0.000		caudal cuneus gyrus	0.000
	posterior parietal thalamus	0.000		rostral lingual gyrus	0.000
	occipital thalamus	0.000		ventromedial parietooccipital sulcus	0.000
	caudal temporal thalamus	0.000		lateral amygdala	0.000
	lateral pre-frontal thalamus	0.000		rostral hippocampus	0.000
				caudal hippocampus	0.000
				ventral caudate	0.000
				medial pre-frontal thalamus	0.000
				rostral temporal thalamus	0.000
				posterior parietal thalamus	0.000
				occipital thalamus	0.000
				caudal temporal thalamus	0.000
				lateral pre-frontal thalamus	0.000

Table 5. Brain regions with statistically significant differences in ADC values between alcohol consumption and no alcohol consumption groups. The Wilcoxon test was used for two-group comparisons. The *P*-values were corrected using the Bonferroni method.

	GMV		CSFV	
Hemisphere	Region	adjusted_p	Region	adjusted_p
Left	Left Hippocampus	0.000	Left CSF	0.000
	Left Basal Forebrain	0.000	Left Hippocampus	0.000
	Left Middle Occipital Gyrus	0.000	Left Angular Gyrus	0.000
			Left Central Operculum	0.000
			Left Inferior Temporal Gyrus	0.000
			Left Subcallosal Area	0.000
Right	Right Amygdala	0.000	Right CSF	0.000
	Right Basal Forebrain	0.000	Right Calcarine Cortex	0.000
	Right Inferior Occipital Gyrus	0.000	Right Cuneus	0.000
	Right Middle Occipital Gyrus	0.000		
	Right Posterior Orbital Gyrus	0.000		

Table 6. Brain regions with statistically significant differences in gray matter volume and in cerebrospinal fluid volume between alcohol consumption and no alcohol consumption groups. The Wilcoxon test was used for two-group comparisons. The *P*-values were corrected using the Bonferroni method.

Hemisphere	Region	adjusted_p	Hemisphere	Region	adjusted_p
Left	Area anterior 9-46v	0.000	Right	Pirform_Cortex	0.000
	Area_TA2	0.000			
	Medial Belt Complex	0.000			

Table 7. . Brain regions with statistically significant differences in cortical thickness between alcohol consumption and no alcohol consumption groups. The Wilcoxon test was used for two-group comparisons. The *P*-values were corrected using the Bonferroni method.

Correlation of curvature in alcoholics

After controlling for confounding factors, the curvature in 5 brain regions was found to be correlated with the amount of alcohol consumed. These regions included the Frontal_Opercular_Area_2, Area_Posterior Insular_1, and Insular Granular Complex in the left hemisphere, as well as the RetroInsular Cortex and Area_Posterior Insular_1 in the right hemisphere. The curvature in all of these brain regions was negatively correlated with the amount of alcohol consumed. Details can be found in Table 15.

Hemisphere, Left			Hemisphere, Rihgt		
Region	ρ	adjusted_p	Region	ρ	adjusted_p
medial area 10	0.489	0.000	medial area 9	0.482	0.000
dorsal area 44	0.472	0.000	medial area 10	0.558	0.000
opercular area 44	0.515	0.000	opercular area 44	0.487	0.000
ventral area 44	0.467	0.000	ventral area 44	0.569	0.000
area 4(tongue and larynx region)	0.461	0.000	area 4(tongue and larynx region)	0.528	0.000
caudal ventrolateral area 6	0.501	0.000	area 41/42	0.503	0.000
area 41/42	0.527	0.000	TE1.0 and TE1.2	0.469	0.000
TE1.0 and TE1.2	0.491	0.000	rostral area 22	0.552	0.000
anterior superior temporal sulcus	0.575	0.000	anterior superior temporal sulcus	0.656	0.000
medioventral area37	0.468	0.000	intermediate ventral area 20	0.484	0.000
posterior parahippocampal gyrus	0.559	0.000	rostroventral area 20	0.546	0.000
caudal area 7	0.504	0.000	caudoposterior superior temporal sulcus	0.482	0.000
rostroventral area 39(PGa)	0.492	0.000	rostroventral area 40(PFop)	0.506	0.000
rostroventral area 40(PFop)	0.558	0.000	area 31 (Lc1)	0.567	0.000
dorsomedial parietooccipital sulcus(PEr)	0.646	0.000	area 1/2/3(tongue and larynx region)	0.544	0.000
area 31 (Lc1)	0.529	0.000	dorsal area 23	0.600	0.000
area 1/2/3(tongue and larynx region)	0.471	0.000	ventromedial parietooccipital sulcus	0.506	0.000
hypergranular insula	0.514	0.000	lateral superior occipital gyrus	0.470	0.000
ventral dysgranular and granular insula	0.553	0.000			
dorsal granular insula	0.463	0.000			
dorsal dysgranular insula	0.485	0.000			
dorsal area 23	0.622	0.000			
pregenual area 32	0.499	0.000			
subgenual area 32	0.497	0.000			
caudal cuneus gyrus	0.515	0.000			
ventromedial parietooccipital sulcus	0.530	0.000			
area V5/MT +	0.464	0.000			
medial superior occipital gyrus	0.461	0.000			
lateral superior occipital gyrus	0.553	0.000			
rostral hippocampus	0.509	0.000			
caudal hippocampus	0.535	0.000			
ventral caudate	0.470	0.000			

Table 8. Brain regions where ADC values correlate with alcohol consumption. One-tailed partial correlation analysis was employed. Age, history of previous cerebral infarction, history of previous cerebral hemorrhage, hypertension, diabetes, coronary heart disease, and smoking history were initially proposed as control variables. However, the results presented here were obtained prior to actually controlling for these variables. The *P*-values were corrected using the Bonferroni method.

Correlation of sulcal depth in alcoholics

After accounting for confounding factors, the sulcal depth in eight brain regions was determined to be correlated with the amount of alcohol consumed. On the left hemisphere, these regions were the Eighth_Visual_Area, Primary_Motor_Cortex, Frontal_Opercular_Area_2, Area_Posterior Insular_1, and Insular Granular Complex. On the right hemisphere, they were the Middle Temporal_Area, RetroInsular Cortex, and Area_Posterior Insular_1. All of these brain regions demonstrated a negative correlation between their sulcal depth and the amount of alcohol consumed. The detailed information is presented in Table 16.

Discussion

Alcohol consumption is linked to reduced brain volume, with even light to moderate drinking capable of causing brain damage. Alcohol intake is negatively correlated with overall brain volume, regional gray matter volume, and white matter microstructure, with this correlation intensifying as alcohol consumption increases[3]. Numerous studies have established that higher alcohol use and alcohol abuse are associated with reduced cortical and subcortical volumes[26,27]. A case–control study of adolescents highlighted a detrimental association between alcohol use and the integrity of white matter microstructure, with widespread FA alterations observed in those beginning to abuse alcohol. Notably, white matter atrophy and demyelination of the corpus callosum are two of the most significant markers of alcoholism in adults[28].

In our study, our primary study population consisted of long-term chronic drinkers who have not yet developed alcohol dependence or alcohol use disorders. In examining the association between neuroimaging

Hemisphere, Left			Hemisphere, Rihgt		
Region	**ρ**	**adjusted_p**	**Region**	**ρ**	**adjusted_p**
medial area 10	0.525	0.000	medial area 10	0.586	0.000
opercular area 44	0.522	0.000	opercular area 44	0.545	0.000
medial area 14	0.492	0.000	ventral area 44	0.641	0.000
area 4(tongue and larynx region)	0.515	0.000	medial area 14	0.522	0.000
caudal ventrolateral area 6	0.506	0.000	area 4(tongue and larynx region)	0.598	0.000
area 41/42	0.592	0.000	caudal ventrolateral area 6	0.523	0.000
TE1.0 and TE1.2	0.511	0.000	area 41/42	0.550	0.000
anterior superior temporal sulcus	0.582	0.000	TE1.0 and TE1.2	0.500	0.000
medioventral area37	0.599	0.000	rostral area 22	0.555	0.000
posterior parahippocampal gyrus	0.579	0.000	anterior superior temporal sulcus	0.634	0.000
caudal area 7	0.520	0.000	intermediate ventral area 20	0.526	0.000
rostroventral area 40(PFop)	0.601	0.000	rostroventral area 20	0.526	0.000
dorsomedial parietooccipital sulcus(PEr)	0.704	0.000	rostroventral area 40(PFop)	0.559	0.000
area 31 (Lc1)	0.603	0.000	area 31 (Lc1)	0.604	0.000
area 2	0.498	0.000	area 1/2/3(tongue and larynx region)	0.572	0.000
hypergranular insula	0.597	0.000	hypergranular insula	0.564	0.000
ventral dysgranular and granular insula	0.570	0.000	dorsal granular insula	0.550	0.000
dorsal granular insula	0.514	0.000	dorsal area 23	0.585	0.000
dorsal area 23	0.618	0.000			
subgenual area 32	0.526	0.000			
rostral cuneus gyrus	0.499	0.000			
caudal cuneus gyrus	0.515	0.000			
ventromedial parietooccipital sulcus	0.544	0.000			
lateral superior occipital gyrus	0.541	0.000			
rostral hippocampus	0.572	0.000			
caudal hippocampus	0.592	0.000			
occipital thalamus	0.524	0.000			

Table 9. . Brain regions where ADC values correlate with alcohol consumption. Age, history of previous cerebral infarction, history of previous cerebral hemorrhage, hypertension, diabetes, coronary heart disease, and smoking history were set as control variables. The *P*-values were corrected using the Bonferroni method.

measures and alcohol use, gray matter volume and white matter volume were reduced in alcoholics, while cerebrospinal fluid volume and cerebral white matter high signal volume were increased. Previous research has also shown similar trends in these brain volume changes among alcohol-consuming populations. However, our study further differentiates by focusing on a population without overt alcohol-use disorders, providing insights into the early-stage effects of long-term alcohol consumption on the brain structure.

In our study, cortical thickness, curvature, and sulcal depth all showed negative correlations with alcohol consumption. This indicates that as alcohol intake rises, these structural features of the brain tend to decrease correspondingly. We also found that the brain regions where cortical thickness is correlated with alcohol consumption are mainly concentrated in the frontal lobe, temporal lobe, insular lobe, and the medial surface of the brain. These regions play crucial roles in functions such as sensation, movement, language, memory, and emotion. A previous study involving 436 twin individuals found that genetic susceptibility to alcohol exposure and alcohol use led to reduced cortical thickness in several regions[29]. Our findings not only validate the decrease in cortical thickness but also pinpoint specific regions that are more severely impacted within our group of long-term drinkers. By demonstrating the regional specificity of these alterations in a distinct study population, our results contribute to the existing body of knowledge.

Employing Neuromorphometrics mapping, our study carried out a more detailed segmentation of the gray matter and cerebrospinal fluid throughout the entire brain. In alcoholics, the structural brain changes mainly affected the orbital surface of the frontal lobe, including the bilateral gyrus rectus, the right lateral orbital gyrus, and the right posterior orbital gyrus; the limbic system, such as the bilateral amygdala, bilateral hippocampus, the middle and posterior parts of the left cingulate gyrus; the bilateral brainstem; the bilateral fusiform gyrus; the left caudate nucleus; the left thalamus; the left inferior temporal gyrus; the bilateral cerebellum; bilateral CSF regions and the bilateral fourth ventricles. Previous research has shown that higher alcohol consumption is associated with an increased risk of hippocampal atrophy in a dose-dependent manner. Even moderate drinkers (14–21 units/week) were three times more likely to experience right hippocampal atrophy compared to non-drinkers. Higher alcohol use has also been linked to differences in corpus callosum microstructure and a rapid decline in lexical fluency[30]. The thalamus, limbic system, cerebellum, and particularly the frontal lobe, are more vulnerable to alcohol-related brain damage than other brain regions. The limbic system primarily includes the

Alcohol consumption		
Region	**ρ**	**adjusted_p**
Left 4th Ventricle	0.608	0.000
Left Amygdala	−0.523	0.000
Left Brainstem	0.564	0.000
Left Cerebellum White Matter	0.500	0.000
Left Hippocampus	−0.473	0.000
Left Entorhinal Area	−0.532	0.000
Right 4th Ventricle	0.619	0.000
Right Brainstem	0.572	0.000
Right Entorhinal Area	−0.529	0.000
Right Fusiform Gyrus	−0.548	0.000
Right Gyrus Rectus	−0.507	0.000

Table 10. Brain regions where gray matter volume correlates with alcohol consumption. One-tailed partial correlation analysis was employed. Age, history of previous cerebral infarction, history of previous cerebral hemorrhage, hypertension, diabetes, coronary heart disease, and smoking history were initially proposed as control variables. However, the results presented here were obtained prior to actually controlling for these variables. The *P*-values were corrected using the Bonferroni method.

Alcohol consumption		
Region	**ρ**	**adjusted_p**
Right Accumbens	0.708	0.000
Left Hippocampus	0.620	0.000
Left Posterior Insula	0.485	0.000
Right Posterior Orbital Gyrus	0.494	0.000
Left Planum Polare	0.523	0.000

Table 11. Brain regions where gray matter volume correlates with alcohol consumption. Age, history of previous cerebral infarction, history of previous cerebral hemorrhage, hypertension, diabetes, coronary heart disease, and smoking history were set as control variables. The *P*-values were corrected using the Bonferroni method.

nucleus ambiguus, amygdala, and hypothalamus[31]. Alcohol consumption leads to a reduction in cortical gray matter volume, particularly in the dorsolateral prefrontal cortex (DLPFC) and premotor cortex[32]. In comparison with previous research, our detailed mapping of the brain regions affected by alcohol offers a more comprehensive perspective on the spatial distribution of alcohol-induced structural alterations. This enhanced understanding can facilitate a more accurate comprehension of the functional implications of alcohol-related brain damage. Given that different brain regions are associated with specific cognitive and emotional functions, our findings contribute significantly to elucidating how alcohol consumption impacts various aspects of brain function.

These brain structures play an integral role in functions including memory, judgment, abstract thinking, cognition, emotion, and impulsive behavior. The amygdala, a central hub in the subcortical region, has been linked to various psychiatric disorders, including anxiety disorders (such as post-traumatic stress disorder, phobias, and panic), depression, schizophrenia, and autism[33]. Additionally, the amygdala forms extensive circuits with the medial prefrontal cortex, orbitofrontal cortex, and hippocampus, mediating abnormal social functioning through complex interactions[34]. The medial frontal cortex is believed to govern cognitive functions, including thinking and perception, and is closely associated with memory, problem-solving, and emotions. It is intricately connected to the limbic system, particularly the amygdala, orbitofrontal cortex, and hippocampus[35–37]. Stimulation of the insula can disrupt visceral functions, causing symptoms such as nausea, belching, increased gastrointestinal motility, or fullness. The anterior insula is involved in olfactory, gustatory, and limbic functions, while the posterior insula is associated with auditory and autonomic sensory-motor functions, as well as addiction[38–41].

Patients with chronic alcohol consumption frequently present symptoms such as anxiety, dysphoria, depressed mood, insomnia, nausea, vomiting, sweating, palpitations, agitation, and tremors. Notably, these symptoms closely resemble those resulting from the structural lesions mentioned above.

In our study, even though the alcoholics had not yet shown obvious cognitive impairment, their Mini-Mental State Examination (MMSE) and Montreal Cognitive Assessment (MoCA) scores were lower compared to those of non-alcoholics. This finding reflected the impaired functions in the frontal lobes and hippocampus[42,43]. Zhao et al. (2024) explored the molecular mechanisms of alcohol-induced neurotoxicity and its role in Alzheimer's disease pathology[44].

Alcohol consumption		
Region	**ρ**	**adjusted_p**
Left Caudate	0.481	0.000
Left Hippocampus	0.627	0.000
Left Thalamus Proper	0.463	0.000
Left Inferior Temporal Gyrus	0.478	0.000
Left Middle Cingulate Gyrus	0.461	0.000
Left Posterior Insula	0.470	0.000
Left Planum Polare	0.528	0.000
Right Accumbens	0.689	0.000
Right Lateral Orbital Gyrus	0.473	0.000
Right Posterior Orbital Gyrus	0.510	0.000

Table 12. Brain regions where cerebrospinal fluid volume correlates with alcohol consumption. One-tailed partial correlation analysis was employed. Age, history of previous cerebral infarction, history of previous cerebral hemorrhage, hypertension, diabetes, coronary heart disease, and smoking history were initially proposed as control variables. However, the results presented here were obtained prior to actually controlling for these variables. The *P*-values were corrected using the Bonferroni method.

Alcohol consumption		
Region	**ρ**	**adjusted_p**
Right Accumbens	0.708	0.000
Left Hippocampus	0.620	0.000
Left Posterior Insula	0.485	0.000
Right Posterior Orbital Gyrus	0.494	0.000
Left Planum Polare	0.523	0.000

Table 13. Brain regions where cerebrospinal fluid volume correlates with alcohol consumption. Age, history of previous cerebral infarction, history of previous cerebral hemorrhage, hypertension, diabetes, coronary heart disease, and smoking history were set as control variables. The *P*-values were corrected using the Bonferroni method.

	Alcohol consumption		
Hemisphere	**Region**	**ρ**	**adjusted_p**
Left	Area_3a	−0.584	0.000
	Area_43	−0.553	0.000
	Area_52	−0.535	0.000
	Posterior Insular Area 2	−0.503	0.000
	Area_TA2	−0.541	0.000
	Frontal Opercular_Area 1	−0.484	0.000
	Area_Posterior Insular_1	−0.513	0.000
	Medial Belt Complex	−0.553	0.000
	Para-Insular_Area	−0.507	0.000
Right	Area_3a	−0.513	0.000
	Area_52	−0.487	0.000
	Area_TA2	−0.493	0.000
	Para-Insular_Area	−0.489	0.000

Table 14. Brain regions where cortical thickness correlates with alcohol consumption. Age, history of previous cerebral infarction, history of previous cerebral hemorrhage, hypertension, diabetes, coronary heart disease, and smoking history were set as control variables. The *P*-values were corrected using the Bonferroni method.

The ADC value reflects the diffusion rate of water molecules, indirectly indicating changes in microstructure and the movement of water molecules within the extracellular matrix[45]. The Brownian motion of water molecules is inversely proportional to cellular tissue density, and the DWI signal is inversely proportional to tissue integrity[46].

	Alcohol consumption		
Hemisphere	Region	ρ	adjusted_p
Left	Frontal_Opercular_Area_2	−0.500	0.000
	Area_Posterior Insular_1	−0.544	0.000
	Insular Granular Complex	−0.477	0.000
Right	RetroInsular Cortex	−0.480	0.000
	Area_Posterior Insular_1	−0.464	0.000

Table 15. Brain regions where curvature correlates with alcohol consumption. Age, history of previous cerebral infarction, history of previous cerebral hemorrhage, hypertension, diabetes, coronary heart disease, and smoking history were set as control variables. The *P*-values were corrected using the Bonferroni method.

	Alcohol consumption		
Hemisphere	Region	ρ	adjusted_p
Left	Eighth_Visual_Area	−0.508	0.000
	Primary_Motor_Cortex	−0.474	0.000
	Frontal_Opercular_Area_2	−0.500	0.000
	Area_Posterior Insular_1	−0.544	0.000
	Insular Granular Complex	−0.477	0.000
Right	Middle Temporal_Area	−0.477	0.000
	RetroInsular Cortex	−0.480	0.000
	Area_Posterior Insular_1	−0.464	0.000

Table 16. Brain regions where sulcal depth correlates with alcohol consumption. Age, history of previous cerebral infarction, history of previous cerebral hemorrhage, hypertension, diabetes, coronary heart disease, and smoking history were set as control variables. The *P*-values were corrected using the Bonferroni method.

The apparent diffusion coefficient (ADC) in various brain regions was quantified by means of a semi-automated processing program. In our study, we utilized the Brainnetome Atlas to divide the brain into 246 regions. We observed that, across these regions, the apparent diffusion coefficient (ADC) values in alcoholics were consistently higher than those in non-alcoholics. Statistical analysis revealed significant differences in 134 of these regions, which was substantially more than the number of regions showing gray matter alterations. This finding suggests that changes in water molecule diffusion within the brains of alcoholics may occur prior to alterations in gray matter. Previous studies have also suggested that the brain MRI apparent diffusion coefficient (ADC) reflects increased hydrogen movement in areas of neurodegeneration, with pathological changes in the shell nuclei detectable as elevated ADC even in the early stages of MSA-P[47]. These findings are consistent with our results. Wang et al. (2024) used diffusion tensor imaging to study the impact of chronic alcohol intake on cognitive function and brain microstructure. They found that chronic alcohol intake was associated with cognitive decline and alterations in brain microstructure, which is also consistent with our results[48].

In contrast to previous studies, our research does not solely focus on directly observing the structural changes in the brain's gray and white matter induced by long-term alcohol consumption. Instead, we also direct our attention to the influence of alcohol on the brain's microstructure and water molecule diffusion, as assessed by Apparent Diffusion Coefficient (ADC) values. By doing so, we explore the early-stage changes from a microscopic viewpoint. Regarding research methods, previous investigations may have utilized relatively simple or traditional brain atlases, which divided the brain into a smaller number of regions. In our study, however, we employ the Brainnetome Atlas to partition the brain into 246 regions. This allows for a more detailed analysis of regional variations, enabling us to detect subtle differences and relationships that might have been overlooked in prior research. This approach not only offers a more comprehensive understanding of the effects of alcohol on the brain but also contributes to a more in-depth exploration of the underlying mechanisms of alcohol-related brain alterations.

In alcoholics, the apparent diffusion coefficient (ADC) values showed a positive correlation with alcohol consumption. The increase in ADC values can likely be ascribed to several factors. These include a reduction in tissue density, a decrease in the volumes of both gray and white matter, an expansion in cerebrospinal fluid volume, and the infiltration of cerebrospinal fluid into the brain parenchyma. The influx of cerebrospinal fluid into the brain has been shown to enhance free water diffusion, thereby increasing ADC[49]. In fetuses and neonates, as the brain matures, there is an increase in lipid content and tissue density, the formation of new synapses, and the bundling of fibrous tissue, all of which correspond with decreased water content and a gradual reduction in water diffusion rates[50].

Cerebral blood flow (CBF) plays a pivotal role in maintaining brain function and is closely linked to structural changes in the brain. Intracranial vascular characteristics, such as vessel radius and length, serve as indicators of cerebral blood flow[13]. In subjects with deep subcortical lesions, significantly increased capillary wall thickness

and decreased capillary density have been observed, both of which contribute to reduced cerebral blood flow[51]. Additionally, a study found that mice in the high-alcohol group had significantly smaller blood vessel diameters compared to their low-alcohol counterparts in weight-matched pairs[52].

While alterations in CBF have been linked to various neurological disorders, including stroke and dementia, chronic reductions in CBF may contribute to brain atrophy and increased signaling in white matter[53]. In patients with Alzheimer's disease, reductions in CBF within the cortical gray matter primarily affect the parietal and temporal lobes, with microstructural abnormalities predominantly observed in the parietal, temporal, and frontal lobes. Lower CBF values in the left occipital lobe, left frontal lobe, and right parietal lobe have been associated with higher mean diffusivity (MD), lower fractional anisotropy (FA), or lower mean kurtosis (MK) values[54]. In white matter, CBF has shown a positive correlation with subject anisotropy scores in the corpus callosum, right posterior thalamic radiation, right inferior fronto-occipital fasciculus, right inferior longitudinal fasciculus, and right superior longitudinal fasciculus. Additionally, radial diffusivity is negatively correlated with CBF in similar regions, and a positive correlation exists between CBF and FA within the inner white matter bundle[55]. Studies of patients with ketonuria have also demonstrated that white matter lesions are associated with reduced cerebral blood flow, particularly in the occipital lobe, where CBF to the left posterior cerebral artery is significantly diminished[56].

Relatively few studies have been dedicated to quantifying the cerebrovascular morphology in alcoholics. In our research, we utilized 3D-Time-Of-Flight Magnetic Resonance Angiography (3D-TOF MRA) to acquire vascular information. Subsequently, image processing techniques were employed to quantify relevant characteristics of the intracranial distal arteries in alcoholics, such as the mean arterial density, mean arterial radius, and mean arterial length. The analysis indicated that in alcoholics, the mean arterial density, mean arterial radius, and mean arterial tortuosity were lower, while the mean arterial flexibility was higher. There was no significant difference in mean vessel length. Notably, a positive correlation was found between gray matter volume and mean arterial length, density, and radius, with significant associations. Similarly, white matter volume demonstrated a positive correlation with mean arterial length and density, with significant correlations. However, the positive correlation between white matter volume and mean arterial radius was not significant. In contrast, the cerebrospinal fluid volume (CSFV) was negatively correlated with mean arterial length and density. Although there was a negative correlation between CSFV and arterial radius, it was not highly pronounced. This gives rise to the hypothesis that the altered cerebrovascular morphology in alcoholics serves as a contributing factor to the alcohol-induced structural changes in the brain. Zhang et al. (2023) also explored the association between cerebrovascular changes and alcohol-related brain damage in a longitudinal study. Their findings support our hypothesis that altered cerebrovascular morphology is a contributing factor to alcohol-induced structural changes in the brain[57].

The MRI biomarkers identified in our study hold substantial clinical significance. In the brains of alcoholics, elevated ADC values, which are observable in numerous regions, can function as an early indicator of alcohol-related brain damage. They might signal the onset of early neurodegeneration even before gray matter alterations become visually detectable, thus enabling the early detection of damage for timely intervention.

The changes in cerebrovascular features, such as decreased arterial density, radius, and length, also bear clinical relevance. These alterations are associated with modified cerebral blood flow, which can contribute to brain structural changes. Measuring these vascular biomarkers can assist clinicians in understanding disease mechanisms and devising more effective treatments.

For the utilization of these biomarkers in diagnosis, it is advisable to implement a comprehensive MRI protocol that includes DWI, T1-weighted, T2-weighted, and MRA sequences for patients under suspicion. Advanced image processing techniques can be employed to extract these biomarkers. By combining them with clinical evaluations, more accurate diagnoses and prognoses can be achieved.

Clinicians can utilize these biomarkers to screen high-risk individuals, such as heavy drinkers, and to monitor the progression of brain damage over time. Additionally, these biomarkers can be used to assess the efficacy of interventions, like alcohol cessation programs. If, following a period of intervention, an individual demonstrates an improvement in these biomarker values, it may suggest a positive response to the treatment.

This study has several limitations.

First, being a cross-sectional study, it provides only a static snapshot of the brain's structural and vascular morphological features at a single point in time. Without dynamic follow-up, we cannot observe how these features evolve over time.

Second, the sample size in our study is relatively small. This may have impeded our ability to detect some potential relationships between vascular morphological features and structural brain changes. A larger and more diverse sample would be required to confirm and generalize our findings.

Third, due to the fact that our examination room does not routinely perform more advanced diffusion-weighted imaging techniques, this study relied solely on the Apparent Diffusion Coefficient (ADC) value to represent the diffusion coefficient of water molecules. For example, Diffusion Tensor Imaging (DTI), which could provide more comprehensive diffusion-related information, is not part of our standard examination protocol. Consequently, we were unable to use these techniques to gain a deeper understanding of the brain's microstructural changes related to water molecule diffusion.

Fourth, the accuracy of Magnetic Resonance Angiography (MRA) in evaluating terminal small vessels is inherently limited. In the hospital where this study was conducted, many MRA-based microvascular assessment items, as well as imaging techniques such as arterial spin labeling (ASL) and dynamic susceptibility contrast (DSC) perfusion MRI, are not yet available. As a result, our study had to rely solely on MRA to obtain the morphological characteristics of distal intracranial arteries. We were restricted to examining segments M2, M3, and M4 of the Middle Cerebral Artery (MCA), segments A2, A3, and A4 of the Anterior Cerebral Artery (ACA), and segments P2, P3, and P4 of the Posterior Cerebral Artery (PCA). This constrained approach, due to the

lack of more comprehensive techniques, may reduce the accuracy of measurements related to vessel volume, curvature, and other crucial parameters.

Fifth, the Neuromorphometrics mapping used in this study only differentiates between different regions of gray matter and cerebrospinal fluid, excluding white matter from its scope.

Finally, the techniques for voxel-based structural MRI analysis and the assessment of intracranial vessel morphological characteristics via MRA are not yet widely used in clinical practice. This lack of widespread implementation, combined with the unavailability of relevant examination items in our facility, severely restricts their current practical application in real-world medical settings.

Nevertheless, we are committed to overcoming these limitations in our future research. This will involve conducting longitudinal studies to track changes over time, significantly increasing the sample sizes to enhance statistical power and generalizability, and exploring more advanced imaging modalities. By doing so, we aim to achieve a more comprehensive and in-depth understanding of the research topic.

Conclusion

The diffusion of water molecules in the brains of alcoholics is modified before any detectable alterations in gray matter structure occur. In chronic alcoholics, cerebrovascular morphological features, including mean arterial density, mean arterial radius, and mean arterial length, are strongly correlated with structural changes in the brain. These changes in cerebrovascular morphology are regarded as a contributing factor to the structural alterations seen in the brains of chronic alcoholics.

Data availability

Data is provided within the manuscript and supplementary information files, further inquiries can be directed to the corresponding author Jia Yanjie.

Received: 13 December 2024; Accepted: 18 June 2025
Published online: 02 July 2025

References

1. Zou, X., Durazzo, T. C. & Meyerhoff, D. J. Regional brain volume changes in alcohol-dependent individuals during short-term and long-term abstinence. *Alcohol Clin. Exp. Res.* **42**(6), 1062–1072. https://doi.org/10.1111/acer.13757 (2018).
2. Bühler, M. & Mann, K. Alcohol and the human brain: A systematic review of different neuroimaging methods. *Alcohol Clin. Exp. Res.* **35**(10), 1771–1793. https://doi.org/10.1111/j.1530-0277.2011.01540.x (2011).
3. Daviet, R. et al. Associations between alcohol consumption and gray and white matter volumes in the UK Biobank. *Nat. Commun.* **13**(1), 1175. https://doi.org/10.1038/s41467-022-28735-5 (2022).
4. Zhou, X. et al. Long-term alcohol consumption and brain atrophy: A meta-analysis of structural MRI studies. *J. Neurol. Sci.* **456**, 120056. https://doi.org/10.1016/j.jns.2024.120056 (2024).
5. Pfefferbaum, A. et al. Adolescent development of cortical and white matter structure in the NCANDA sample: Role of sex, ethnicity, puberty, and alcohol drinking. *Cereb. Cortex.* **26**(10), 4101–4121. https://doi.org/10.1093/cercor/bhv205 (2016).
6. Topiwala, A., Ebmeier, K. P., Maullin-Sapey, T. & Nichols, T. E. Alcohol consumption and MRI markers of brain structure and function: Cohort study of 25,378 UK Biobank participants. *Neuroimage Clin.* **35**, 103066. https://doi.org/10.1016/j.nicl.2022.103066 (2022).
7. Ashburner, J. & Friston, K. J. Voxel-based morphometry—The methods. *Neuroimage* **11**(6 Pt 1), 805–821. https://doi.org/10.1006/nimg.2000.0582 (2000).
8. Dale, A. M., Fischl, B. & Sereno, M. I. Cortical surface-based analysis. I. Segmentation and surface reconstruction. *Neuroimage* **9**(2), 179–194. https://doi.org/10.1006/nimg.1998.0395 (1999).
9. Jenkinson, M., Beckmann, C. F., Behrens, T. E., Woolrich, M. W. & Smith, S. M. FSL. *Neuroimage* **62**(2), 782–790. https://doi.org/10.1016/j.neuroimage.2011.09.015 (2012).
10. Fan, L. et al. The human brainnetome atlas: A new brain atlas based on connectional architecture. *Cereb. Cortex.* **26**(8), 3508–3526. https://doi.org/10.1093/cercor/bhw157 (2016).
11. Qi, Q. et al. Morphological changes of cerebral vessels and expression patterns of MMP-2 and MMP-9 on cerebrovascular wall of alcoholic rats. *Int. J. Clin. Exp. Pathol.* **7**(5), 1880–1888 (2014).
12. Liu, X. et al. Progressive mechanical and structural changes in anterior cerebral arteries with Alzheimer's disease. *Alzheimers Res. Ther.* **15**(1), 185. https://doi.org/10.1186/s13195-023-01331-5 (2023).
13. Cheng, H. et al. Association between morphologic features of intracranial distal arteries and brain atrophy indexes in cerebral small vessel disease: A voxel-based morphometry study. *Front. Neurol.* **14**, 1198402. https://doi.org/10.3389/fneur.2023.1198402 (2023).
14. Edelman, R. R. & Koktzoglou, I. Noncontrast MR angiography: An update. *J. Magn. Reson. Imaging.* **49**(2), 355–373. https://doi.org/10.1002/jmri.26288 (2019).
15. Gao, X. et al. A fast and fully automatic method for cerebrovascular segmentation on time-of-flight (TOF) MRA image. *J. Digit. Imaging.* **24**(4), 609–625. https://doi.org/10.1007/s10278-010-9326-1 (2011).
16. Chen, L. et al. Quantification of morphometry and intensity features of intracranial arteries from 3D TOF MRA using the intracranial artery feature extraction (iCafe): A reproducibility study. *Magn. Reson. Imaging.* **57**, 293–302. https://doi.org/10.1016/j.mri.2018.12.007 (2019).
17. Wang, X. et al. Skeleton-based cerebrovascular quantitative analysis. *BMC Med. Imaging.* **16**(1), 68. https://doi.org/10.1186/s12880-016-0170-8 (2016).
18. Deshpande, A. et al. Automatic segmentation, feature extraction and comparison of healthy and stroke cerebral vasculature. *Neuroimage Clin.* **30**, 102573. https://doi.org/10.1016/j.nicl.2021.102573 (2021).
19. Fedorov, A. et al. 3D slicer as an image computing platform for the quantitative imaging network. *Magn. Reson. Imaging.* **30**(9), 1323–1341. https://doi.org/10.1016/j.mri.2012.05.001 (2012).
20. Mandolini, M. et al. Comparison of three 3D segmentation software tools for hip surgical planning. *Sensors (Basel).* **22**(14), 5242. https://doi.org/10.3390/s22145242 (2022).
21. Rehm, J. The risks associated with alcohol use and alcoholism. *Alcohol Res. Health.* **34**(2), 135–143 (2011).
22. China Nutrition Society. Dietary Guidelines for Chinese Residents (2022 Edition). People's Medical Publishing House, 2022.
23. Wang, L. M. et al. Epidemiological study on alcohol consumption and agricultural profession-related injuries among minority residents from the northern parts of China. *Zhonghua Liu Xing Bing Xue Za Zhi* **30**(12), 1252–1257 (2009) (**in Chinese**).

24. Saunders, J. B., Aasland, O. G., Babor, T. F., de la Fuente, J. R. & Grant, M. Development of the alcohol use disorders identification test (AUDIT): WHO collaborative project on early detection of persons with harmful alcohol consumption-II. *Addiction* **88**(12), 1795–1805. https://doi.org/10.1111/j.1360-0443.1993.tb02093.x (1993).
25. Glasser, M. F. et al. A multi-modal parcellation of human cerebral cortex. *Nature* **536**(7615), 171–178. https://doi.org/10.1038/nature18933 (2016).
26. Baranger, D. A. A. et al. Convergent evidence for predispositional effects of brain gray matter volume on alcohol consumption. *Biol. Psychiatry.* **87**(7), 645–655. https://doi.org/10.1016/j.biopsych.2019.08.029 (2020).
27. Hatoum, A. S., Johnson, E. C., Agrawal, A. & Bogdan, R. Brain structure and problematic alcohol use: A test of plausible causation using latent causal variable analysis. *Brain Imaging Behav.* **15**(6), 2741–2745. https://doi.org/10.1007/s11682-021-00482-z (2021).
28. Zhao, Q. et al. Association of heavy drinking with deviant fiber tract development in frontal brain systems in adolescents. *JAMA Psychiat.* **78**(4), 407–415. https://doi.org/10.1001/jamapsychiatry.2020.4064 (2021).
29. Harper, J. et al. The effects of alcohol and cannabis use on the cortical thickness of cognitive control and salience brain networks in emerging adulthood: A co-twin control study. *Biol. Psychiatry.* **89**(10), 1012–1022. https://doi.org/10.1016/j.biopsych.2021.01.006 (2021).
30. Topiwala, A. et al. Moderate alcohol consumption as risk factor for adverse brain outcomes and cognitive decline: Longitudinal cohort study. *BMJ* **357**, j2353. https://doi.org/10.1136/bmj.j2353 (2017).
31. Kong, L. M., Zeng, J. Y., Zheng, W. B., Shen, Z. W. & Wu, R. H. Effects of acute alcohol consumption on the human brain: Diffusional Kurtosis imaging and arterial spin-labeling study. *AJNR Am. J. Neuroradiol.* **40**(4), 641–647. https://doi.org/10.3174/ajnr.A5992 (2019).
32. Morris, L. S., Dowell, N. G., Cercignani, M., Harrison, N. A. & Voon, V. Binge drinking differentially affects cortical and subcortical microstructure. *Addict. Biol.* **23**(1), 403–411. https://doi.org/10.1111/adb.12493 (2018).
33. LeDoux, J. The amygdala. *Curr. Biol.* **17**(20), R868–R874. https://doi.org/10.1016/j.cub.2007.08.005 (2007).
34. Meisner, O. C., Nair, A. & Chang, S. W. C. Amygdala connectivity and implications for social cognition and disorders. *Handb. Clin. Neurol.* **187**, 381–403. https://doi.org/10.1016/B978-0-12-823493-8.00017-1 (2022).
35. Vaidya, A. R. & Fellows, L. K. Ventromedial frontal lobe damage affects interpretation, not exploration, of emotional facial expressions. *Cortex* **113**, 312–328. https://doi.org/10.1016/j.cortex.2018.12.013 (2019).
36. de la Vega, A., Chang, L. J., Banich, M. T., Wager, T. D., Yarkoni, T. Large-scale meta-analysis of human medial frontal cortex reveals tripartite functional organization. *J. Neurosci.* **36**(24), 6553–6562. https://doi.org/10.1523/JNEUROSCI.4402-15.2016 (2016). Erratum in: *J. Neurosci*. 37(13):3735. https://doi.org/10.1523/JNEUROSCI.0471-17.2017 (2017).
37. Minxha, J., Adolphs, R., Fusi, S., Mamelak, A. N. & Rutishauser, U. Flexible recruitment of memory-based choice representations by the human medial frontal cortex. *Science* **368**(6498), eaba3313. https://doi.org/10.1126/science.aba3313 (2020).
38. Ellingsen, D. M. et al. Cyclic vomiting syndrome is characterized by altered functional brain connectivity of the insular cortex: A cross-comparison with migraine and healthy adults. *Neurogastroenterol. Motil.* **29**(6), 2. https://doi.org/10.1111/nmo.13004 (2017).
39. Haaranen, M. et al. Anterior insula stimulation suppresses appetitive behavior while inducing forebrain activation in alcohol-preferring rats. *Transl. Psychiatry.* **10**(1), 150. https://doi.org/10.1038/s41398-020-0833-7 (2020).
40. Nicolas, C. et al. Linking emotional valence and anxiety in a mouse insula-amygdala circuit. *Nat. Commun.* **14**(1), 5073. https://doi.org/10.1038/s41467-023-40517-1 (2023).
41. Roquet, D. & Conti, F. Disentangling the association between the Insula and the autonomic nervous system. *J. Neurosci.* **41**(14), 3051–3053. https://doi.org/10.1523/JNEUROSCI.2225-20.2021 (2021).
42. Sui, H., Yang, J., Xiang, H. & Yan, C. Combining ADC values in DWI with rCBF values in arterial spin labeling (ASL) for the diagnosis of mild cognitive impairment (MCI). *Medicine (Baltimore)* **102**(37), e34979. https://doi.org/10.1097/MD.0000000000034979 (2023).
43. Tao, J. et al. Mind-body exercise improves cognitive function and modulates the function and structure of the hippocampus and anterior cingulate cortex in patients with mild cognitive impairment. *Neuroimage Clin.* **23**, 101834. https://doi.org/10.1016/j.nicl.2019.101834 (2019).
44. Zhao, Y. et al. Molecular mechanisms of alcohol-induced neurotoxicity and its role in Alzheimer's disease pathology. *J. Neurosci. Res.* **102**(8), 1521–1533. https://doi.org/10.1002/jnr.25340 (2024).
45. Han, Y., Wu, P., Tian, J., Chen, H. & Yang, C. Diffusion Kurtosis imaging and diffusion weighted imaging comparison in diagnosis of early hypoxic-ischemic brain edema. *Eur. J. Med. Res.* **28**(1), 159. https://doi.org/10.1186/s40001-023-01090-x (2023).
46. Lindt, B., Richter, H. & Del Chicca, F. Investigated regional apparent diffusion coefficient values of the morphologically normal feline brain. *J. Feline Med. Surg.* **24**(8), e214–e222. https://doi.org/10.1177/1098612X221101535 (2022).
47. Umemura, A. et al. Diagnostic accuracy of apparent diffusion coefficient and 123I-metaiodobenzylguanidine for differentiation of multiple system atrophy and Parkinson's disease. *PLoS ONE* **8**(4), e61066. https://doi.org/10.1371/journal.pone.0061066 (2013).
48. Wang, Z. et al. Impact of chronic alcohol intake on cognitive function and brain microstructure: A diffusion tensor imaging study. *Alcohol Alcohol.* **59**(2), 193–200. https://doi.org/10.1093/alcalc/agad097 (2024).
49. Demiral, ŞB. et al. Apparent diffusion coefficient changes in human brain during sleep—Does it inform on the existence of a glymphatic system?. *Neuroimage* **185**, 263–273. https://doi.org/10.1016/j.neuroimage.2018.10.043 (2019).
50. Schönberg, N. et al. The influence of various cerebral and extracerebral pathologies on apparent diffusion coefficient values in the fetal brain. *J. Neuroimaging* **30**(4), 477–485. https://doi.org/10.1111/jon.12727 (2020).
51. Tu, M. C., Chung, H. W., Hsu, Y. H., Yang, J. J. & Wu, W. C. Stage-dependent cerebral blood flow and leukoaraiosis couplings in subcortical ischemic vascular disease and Alzheimer's disease. *J. Alzheimers Dis.* **86**(2), 729–739. https://doi.org/10.3233/JAD-215405 (2022).
52. Mozumder, M. et al. Quantitative histomorphometry of capillary microstructure in deep white matter. *Neuroimage Clin.* **23**, 101839. https://doi.org/10.1016/j.nicl.2019.101839 (2019).
53. Meombe Mbolle, A., Yang, H. & Jiang, H. Photoacoustic imaging for in vivo quantification of alcohol-induced structural and functional changes in cerebral vasculature in high alcohol-preferring mice (HAP). *Alcohol* **100**, 23–30. https://doi.org/10.1016/j.alcohol.2022.01.001 (2022).
54. Niu, X. et al. The correlation between changes in gray matter microstructure and cerebral blood flow in Alzheimer's disease. *Front. Aging Neurosci.* **15**, 1205838. https://doi.org/10.3389/fnagi.2023.1205838 (2023).
55. Giezendanner, S. et al. Microstructure and cerebral blood flow within white matter of the human brain: A TBSS analysis. *PLoS ONE* **11**(3), e0150657. https://doi.org/10.1371/journal.pone.0150657 (2016).
56. Steiner, L. et al. Cerebral blood flow and white matter alterations in adults with phenylketonuria. *Neuroimage Clin.* **41**, 103550. https://doi.org/10.1016/j.nicl.2023.103550 (2024).
57. Zhang, Y. et al. Association between cerebrovascular changes and alcohol-related brain damage: A longitudinal study. *Stroke Vasc. Neurol.* **8**(4), e000787. https://doi.org/10.1136/svn-2023-000787 (2023).

Acknowledgements

We would like to extend our sincere gratitude to Dr. Binbin Nie from the Chinese Academy of Sciences for her invaluable assistance in the NMR image analysis. Additionally, we are thankful to our colleagues in the Neurology, Laboratory, and Imaging departments. Their contributions have been highly appreciated. Moreover, we are

deeply indebted to the associate editor and the reviewers. Their constructive feedback has significantly enhanced the quality of this paper.

Author contributions

Yanjie Jia conceived the research idea. He provided guidance and supervision during the implementation of the study, offered expert opinions, and reviewed and revised the manuscript. Longbin Jia, Lina Xu, Fengbing Yang, Jinna Li, and Hongjiang Cheng contributed ideas and expert opinions throughout the execution of the study. Huanhuan Cui was in charge of administering all the scales. Jing Guo was responsible for collecting blood specimens, as well as extracting and preserving the serum. Jianqiang Wang and Chong Li oversaw the collection of qualified MRI and 3D-TOF MRA data. Cuiqin Wang was accountable for the detailed experimental design, its execution, data collection, organization, analysis, graphing, and for writing and revising the manuscript.

Declarations

Competing interests

The authors declare no competing interests.

Ethical approval and consent to participate

In accordance with the Declaration of Helsinki, this study was approved by the Ethics Committee of Jincheng City People's Hospital (JCPH.NO20230710004). All participants, or their guardians, provided written informed consent.

Consent for publication

All authors contributed to this article and approved its submission.

Additional information

Supplementary Information The online version contains supplementary material available at https://doi.org/10.1038/s41598-025-07984-6.

Correspondence and requests for materials should be addressed to Y.J.

Reprints and permissions information is available at www.nature.com/reprints.

Publisher's note Springer Nature remains neutral with regard to jurisdictional claims in published maps and institutional affiliations.